Surface available gravitational potential energy in the world oceans

Ruixin Huang[2], Bo Qiu[3], Zhiyou Jing[1]*

[1] State Key Laboratory of Tropical Oceanography, South China Sea Institute of Oceanology, Chinese Academy of Sciences, Guangzhou 510301, China

[2] Woods Hole Oceanographic Institution, Woods Hole, MA 02543, USA

[3] Department of Oceanography, University of Hawaii at Manoa, Honolulu, HI 96822, USA

Abstract

Satellite altimetry observations, including the upcoming Surface Water and Ocean Topography mission, provide snapshots of the global sea surface high anomaly field. The common practice in analyzing these surface elevation data is to convert them into surface velocity based on the geostrophic approximation. With increasing horizontal resolution in satellite observations, sea surface elevation data will contain many dynamical signals other than the geostrophic velocity. A new physical quantity, the available surface potential energy, is conceptually introduced in this study defined as the density multiplied by half of the squared deviation from the local mean reference surface elevation. This gravitational potential energy is an intrinsic property of the sea surface height field and it is an important component of ocean circulation energetics, especially near the sea surface. In connection with other energetic terms, this new variable may help us better understand the dynamics of oceanic circulation, in particular the processes in connection with the free surface data collected through satellite altimetry. The preliminary application of this concept to the numerically generated monthly mean Global Ocean Data Assimilation System data and Archiving, Validation, and Interpretation of Satellite Oceanographic altimeter data shows that the available surface potential energy is potentially linked to other dynamic variables, such as the total kinetic energy, eddy kinetic energy and available potential energy.

Key words: satellite altimetry, surface available potential energy, eddy kinetic energy

---

1 Introduction

Oceanic circulation includes many complicated dynamical processes, and it can be examined through different angles. The oceanic circulation is commonly formulated in terms of conservation of mass and momentum, and this approach is further extended into the conservation of angular momentum and vorticity (or potential vorticity). In addition, energetics is also an import aspect of the circulation. The oceanic circulation, including both the wind-driven circulation and the thermohaline circulation, is a dissipative system. The new paradigm of oceanic circulation claims that ocean is not a heat engine and thus the maintenance of the wind-driven circulation and thermohaline circulation require external sources of mechanical energy. Energetics of the oceanic general circulation include the sources/sinks and their transformation of internal energy, kinetic energy (KE) and gravitational potential energy (GPE).

Over the past two decades, the balance of mechanical energy, including the sources/sinks and their transport and transformation, has been the focus of extensive studies. The commonly discussed forms of mechanical energy include: the KE of the mean flow and eddies, and the GPE of the mean flow and eddies. Although the oceanic general circulation contains a huge amount of GPE, most part of this energy is inert, i.e., they do not take part in the dynamical processes of our concern. Thus, the concept of available potential energy (APE) has been introduced and widely used in many studies.

The basic idea for APE is to separate the GPE into the active and non-active parts, based on identifying GPE associated with horizontal density difference, which is directly linked to the oceanic circulation. Margules (1905) first postulated the basic idea, accordingly a reference state which has the minimal GPE is defined, and the difference in GPE between the physical state and the reference state is defined as the APE for the physical state. However, the application of APE to atmospheric dynamics appeared primarily after Lorenz (1955) introduced an approximate definition of APE.

In oceanography APE is often defined in terms of the Boussinesq approximation, in which the free surface of ocean is replaced by the rigid-lid approximation. Furthermore, searching of the reference state is also a key in calculating the APE. In most studies for the basin-scale oceanic circulation, APE is calculated according to the quasi-geostrophic approximation (Oort et al., 1994, 1989; Pedlosky, 1987; Reid et al., 1981).

$$\chi = \frac{g}{2} \iiint \frac{(\rho - \bar{\rho})^2}{\partial \rho_\theta / \partial z} \mathrm{d}v, \tag{1}$$

where g is the gravity; ρ is the density; $\bar{\rho}$ is the reference density; $\partial \rho_\theta / \partial z$ denotes the vertical gradient of the potential density. The reference state (denoted by the overbar) is defined by horizontal averaging of the density field and the vertical gradient of the horizontal-mean potential density. Although this definition is simple and can provide a sound approximation in the study of mesoscale eddies and baroclinic instability, it is not accurate enough in the study of basin scale wind-driven and thermohaline circulation (Huang, 2005).

The key issue is how to define the reference state. Oort et al. (1989, 1994) used the global mean as the reference state, which is likely not a good choice. In fact, for most cases the mean stratification in the vicinity of the area in concern is defined as the reference state, and the APE so calculated should be called the mesoscale APE as suggested by Huang (2010). APE defined in this way has been examined extensively.

On the other hand, basin-scale circulation is closely linked to stratification change on horizontal scales up to 1 000–10 000 km. For such motions, the suitable reference state should have the global scale, and the relevant calculation of APE was studied by Huang (2005), and a much more accurate calculation of APE should be based on mass conservation, not the Boussinesq approximation used in many other studies.

Although the study of APE over the past decades has been extensive, an important aspect of GPE has been overlooked thus far. Sea water in the world oceans has a free surface, which also changes over broad spatial/temporal scales. In the gravitational field, the movement of free surface is directly linked to the change of GPE. This part of GPE is closely linked to many dynamical processes in the ocean; thus, it should be included in the energetics of the oceanic circulation.

The wind stress at the surface ocean is considered as the major driving force for the sea surface height (SSH) anomaly in the ocean. Wind stress effect on SSH manifests in broad spatial (from mm to 1 000s km) and temporal scales (from seconds to decade); changes in SSH driven by wind stress is directly linked to the dynamical processes of the oceanic general circulation. For example, wind stress drives the surface waves in the upper ocean; in addition, wind stress also drives the Ekman transport in the upper ocean, and the convergence/divergence of the Ekman transport gives rise to the major wind-driven currents in the upper ocean, including the subtropical/subpolar gyres and their associated western boundary currents, the equatorial currents, and multiple fronts associated with the Antarctic Circumpolar Current (Apel, 1980).

As the horizontal scale of oceanographic research is pushed towards higher and higher resolution, the mesoscale eddies and submesoscale currents are the current research frontier. Sea surface elevation signals collected through satellite observations provide rich information of the relevant dynamics. For even higher resolution, surface and internal waves may play important roles. These phenomena have been observed as early as in 1970s (Apel et al., 1975, 1976). Wind stress also drives the surface waves and many dynamical processes, such as the Langmuir circulation. It is worth emphasizing that storms and hurricanes, including their associated sea level atmospheric pressure anomaly and wind stress, are important elements in setting up the SSH anomaly. In addition, internal waves driven by either tidal force or surface wind stress can also affect SSH (Ray and Zaron, 2011;

Zhao, 2017). Oceanic current, mesoscale eddies and submesoscale currents are closely linked to changes in SSH (Qiu et al., 2017; Cao et al., 2019). Furthermore, surface heating/cooling, precipitation/evaporation, river run off, and land-based glacial melting can also affect SSH (Frederikse et al., 2020).

The tradition in oceanic study was to collect data from the ship-board instruments, such as conductivity temperature depth (CTD) and expendable bathythermograph (XBT), and the mooring instruments. However, such methods are slow and time consuming. To collect oceanic data over the global scale satellite observations are much better suited. Since sea water is conductive fluid, measurements from space are mostly confined to the upper surface of the ocean, in particular altimetry data have been widely used over the past decades. The Archiving, Validation, and Interpretation of Satellite Oceanographic (AVISO) altimetric data provides global maps of SSH variability and has revealed that mesoscale eddies are the major oceanic KE reservoir (Ferrari and Wunsch, 2009).

Over the past decades, the AVISO altimetry data has been identified to be very useful for our understanding of ocean dynamics of feature radius scales of about 50 km or above, including the studies of mesoscale eddies, large-scale ocean circulation variability and sea level rise. However, traditional altimeter measurements can only resolve balanced geostrophic processes of $Ro \ll 1$ and miss the submesoscale signals characterized by order one Ro due to gaps between satellite footprints (Chavanne and Klein, 2010). For scales smaller than 50 km, the forthcoming Surface Water and Ocean Topography (SWOT) data is expected to improve our understanding of submesoscale variability. However, for such smaller scales, the traditional way of computing the geostrophic velocity from SSH signal is questionable, as discussed by Chelton et al. (2019). Actually, due to the perceived importance in both lateral and vertical exchanges, submesoscale physics in the upper ocean have received intense study through field observations and simulations especially in the past decade (Klymak et al., 2016; Sullivan and McWilliams, 2018; Taylor and Ferrari, 2011; Thomas et al., 2016; Qiu et al., 2017). These submesoscale processes with horizontal scale much smaller than balanced geostrophic motions are detected to significantly contribute to the physical and biogeochemical budgets of the oceans, including enhanced air-sea communication, nutrient supply for phytoplankton growth, and downscale energy cascade of geostrophic eddies (Gula et al., 2014; Mahadevan, 2016; Su et al., 2018). The new wide-swath altimeter of SWOT mission is expected to provide an unprecedented opportunity to obtain submesoscale resolving SSH data (Chelton et al., 2019), in which both geostrophic and ageostrophic dynamical signals are included. Thus, understanding the SSH signals resulting from different oceanic motions are also important for the analysis and application of the forthcoming SWOT altimeter data.

We emphasize that the SSH signals obtained from satellite observations are the basic quantity both AVISO and SWOT can provide. The important question is what type of information we can extract from the SSH signals? In most previous studies, SSH signals have been examined through different ways of analysis, including wavenumber spectrum of SSH, geostrophic velocity computed from SSH and corresponding vorticity. A major problem in deriving the velocity based on geostrophy is that for the new-generation wide-swath SWOT mission, the horizontal scale is on the order of 10 km. For such a horizontal scale, geostrophy may no longer be a valid assumption (Qiu et al., 2018). In fact, for

horizontal scale of 100 km or less, the SSH signals contain dynamic signals from many types of motions in the ocean, including geostrophic motions, submesoscale ageostrophic motions, internal waves, and internal tides. Thus, the SSH signals should be analyzed from a different angle.

The energy associated with the SSH can be a useful signal for our understanding of the upper ocean dynamics. We believe that the energy associated with the SSH and its connection with other forms of energy, such as the total kinetic energy (TKE), the mean kinetic energy (MKE), the eddy kinetic energy (EKE), and the conversion between these forms of energy are an important part of our understanding of the multiscale circulation in the ocean. There is so far very little study about the energy associated with the SSH, with an exception that in the classical theory of surface waves, it is known that the KE and GPE averaged over the period of the wave are equally partitioned (Mei, 1983). For the world ocean, the total mechanical energy input into the surface waves is huge, on the order of 60 TW (Wang and Huang, 2004). Although most of this energy is dissipated within the upper ocean, a small fraction of this energy can penetrate into the subsurface ocean and affect the oceanic general circulation. The conversion and transportation of the mechanical energy from winds to surface waves remains unclear and it is a grand challenge for the study of the upper ocean dynamics.

This study is organized as follows. In Section 2, we lay down the physical foundation of GPE associated with the sea surface elevation for both the homogeneous fluid and stratified fluid. In particular, the concept of available surface potential energy (ASPE) defined as the density multiplied by half of the squared deviation from the local mean reference surface elevation $(\chi_s = \frac{g\rho_0}{2}(\eta - \bar{\eta})^2)$ is introduced, which can be used as an important physical quantity in the study related to sea surface elevation signals. In Section 3, the concept of surface potential energy (SPE) and ASPE is applied to the multi-year climate simulation of Global Ocean Data Assimilation System (GODAS) data (Behringer and Xue, 2004) and the AVISO data. This preliminary application shows the potential meaning and value of the ASPE. Finally, we conclude in Section 4.

2 Energetics associated with surface potential energy in the ocean

Energetics is a classical topic discussed in many papers and textbooks. In this section we briefly summarize and present a condensed version of energetics in the ocean, with an emphasis on the potential energy associated with the sea surface height.

2.1 *Energetics in a homogeneous ocean*

2.1.1 *Basic equations for a one-layer model*

The basic formulation of one-layer model has been discussed in many papers and textbooks (Blumen, 1972; Gill, 1982; Huang, 2010; Pedlosky, 1987). Our focus here is a model of homogeneous fluid with a free surface. The following equations are formulated for a single layer homogeneous fluid of constant density ρ_0. The dynamical effects of mesoscale eddy and turbulence are parameterized in terms of lateral and bottom frictions in the horizontal momentum equations. The model is subject to wind stress from above, lateral friction and bottom friction. In order to present analytical solutions in concise forms, the model in this section is formulated on a β-plane. Under these assumptions, the momentum and continuity equations are

$$hu_t + huu_x + hvu_y - fhv = -gh\eta_x + \tau^x/\rho_0 + A\nabla_h^2(hu) - \kappa hu, \quad (2)$$

$$hv_t + huv_x + hvv_y + fhu = -gh\eta_y + \tau^y/\rho_0 + A\nabla_h^2(hv) - \kappa hv, \quad (3)$$

$$h_t + (hu)_x + (hv)_y = 0, \quad (4)$$

where u and v are the zonal and meridional velocities, respectively; g is the gravity; f is the Coriolis frequency; η is the surface elevation. $()t$ is the derivative with respect to t (time); $()x$ is the derivative with respect to x (eastward coordinate); $()y$ is the derivative with respect to y (northward coordinate). h is the layer thickness, $\eta = h - h_0$ is the sea surface height anomaly relative to the mean sea surface height h_0, (τ^x, τ^y) are the wind stresses, A is the lateral friction coefficient, and κ is the bottom friction coefficient. Note that here wind stress is treated as a body force for the whole layer.

The vorticity dynamics associated with geostrophic adjustment has been discussed extensively, e.g., Blumen (1972). However, the energetics of the model ocean have not received adequate attention, in particular the potential energy associated with the surface elevation anomaly; thus, our discussion here is focused on this aspect of the adjustment.

Multiplying Eq. (2) by $\rho_0 u$ and Eq. (3) by $\rho_0 v$, and adding the results lead to

$$hK_t + hu(K+p)_x + hv(K+p)_y = W, \quad (5)$$

where $K = \rho_0 \frac{u^2 + v^2}{2}$, $p = \rho_0 g\eta$ are the KE and sea level pressure for the fluid column;

$$W = (u\tau^x + v\tau^y) - \kappa\rho_0 h(u^2 + v^2) + A\rho_0[u\nabla_h^2(hu) + v\nabla_h^2(hv)] \quad (6)$$

is the work associated with wind stress, bottom and lateral friction. Equation (3) can be rewritten as

$$P_t + p(hu)_x + p(hv)_y = 0, \quad P = \frac{\rho_0 g\eta^2}{2}, \quad (7a)$$

$$K\left[h_t + (hu)_x + (hv)_y\right] = 0, \quad (7b)$$

Adding Eqs (5), (7a) and (7b) leads to the final form of energy conservation

$$E_t + (uF)_x + (vF)_y = W, E = hK + P, F = hK + hp, \quad K = \rho_0 \frac{u^2 + v^2}{2}. \quad (8)$$

If there is no flux through the lateral boundaries and no forcing, the total energy should be conserved, i.e. $E = hK + P$ integrated over the model domain should remain constant. F is the energy flux. Here the potential energy is given by P and the potential energy flux is given by hp.

In this simple model ocean, the source of mechanical energy comes from wind stress applied to the surface; the lateral and bottom frictions are the sinks of mechanical energy. If we neglect the wind stress and friction, the total energy is conserved during the motions; thus, the energy is converted between the kinetic and potential energy associated with the free surface.

2.1.2 *The Rossby adjustment of a homogeneous fluid*

The energy conservation and transformation associated with

large-scale (balance) motions of a homogeneous fluid can be examined through analytical models, and these problems are commonly referred to as the Rossby wave adjustment. The details of such adjustment are included in the supplementary materials. When the width of the initial velocity jet is much smaller than the deformation radius, energy in the final state is mostly retained in the original region and in the form of KE associated with the geostrophic velocity, while the potential energy associated with the pressure field consists of a very small portion. The energy dispersed to the originally resting part of the ocean is quite small. When the width of the initial velocity jet is much larger than the deformation radius, most of the original KE is dissipated during the process of geostrophic adjustment.

For the case with an initial step in free surface, the geostrophic velocity field is established after the adjustment. About 1/3 of the ASPE is dispersed to infinity through gravity wave radiation during the adjustment. For the case with an initial finite step of finite width in free surface, when the width of the initial step is much smaller than the deformation radius, the potential energy loss in central region is mostly converted into potential energy gain in the two side regions. This potential energy transport between the central and side regions indicates that there is little energy conversion from the potential energy into KE. When the width of the initial step in free surface is much larger than the deformation radius, change in the free surface elevation is mostly confined to the vicinity of the initial front with the order of deformation radius.

In summary, when the horizontal scale of the initial step perturbation is much smaller than the deformation radius, the pressure field is adjusted toward the velocity field. As a result, surface perturbation is most dispersed, and the potential energy in the initial strip of surface anomaly is mostly transported toward the initially undisturbed region; the velocity and KE in the final state is negligible.

Our discussion above is focused on barotropic fluid, so that the analysis applies to the free surface height anomaly in connection with the tidal force, sea level atmospheric pressure anomaly, wind stress forcing, and barotropic currents in the ocean. For the stratified ocean, the baroclinic effect should be included. For example, precipitation and air-sea heat flux anomaly can induce free surface anomaly which is associated with pressure anomaly in baroclinic forms, e.g., Huang and Jin (2002).

2.2 *On the relation between APE and ASPE*

As shown in Fig. S4, for an idealized two-layer model ocean, assume a uniform geostrophic velocity in the upper layer in the physical state, the available potential energy in this two-layer system is

$$(\chi_1 + \chi_2) - (\chi_{1,0} + \chi_{2,0}) = \chi_{bc} + \chi_s = \frac{g\Delta\rho H^2 b}{6} + \frac{g\rho_0 N^2 b}{6}, \quad (9)$$

where, χ_{bc} and χ_s are the baroclinic APE and the ASPE, H and N are the depth scale and the surface elevation scale, and b is the width of the water column. In general, $\Delta\rho/\rho_0 \sim 0.001$–$0.003$; thus, ASPE is much smaller than APE. However, in a quasi-steady state, the SSH anomaly is directly linked to the slope of the main thermocline; as such, the existence of ASPE is also linked to the existence of APE. Furthermore, the ASPE is directly linked to the surface velocity; thus, it may play a critical role in the upper ocean dynamics.

The ratio of APE vs. KE is

$$\chi_{bc}/K = 12 \left(\frac{h_{10}}{H}\right)\left(\frac{\lambda}{b}\right)^2, \quad (10)$$

where h_{10} and λ are the depth scale and first-mode radius of deformation. If the width of the original jet is much larger than the deformation radius, the APE is much larger than KE.

The discussion in this section is focused on large scale circulation, with horizontal scales on the order of first baroclinic radius of deformation; thus, in the final state after the adjustment the velocity field satisfies the geostrophic constraint. The frontier study related to the SWOT and other means of observation is now in the regime of submesoscale or even finer scale, geostrophy is no longer a valid dynamical constraint, so that other terms in the dynamical balance should be included in the analysis.

3 Available surface potential energy in the world oceans

Large scale motions in the world oceans can be characterized by the near balance of different forms of force and energy. In terms of the force, these motions are approximately in geostrophic balance; in terms of energy the GPE and KE are the most important and active components of the energetics. The APE discussed in previous studies of oceanography is essentially due to the non-uniform distribution of stratification in the ocean. If we omit the stratification and treat the ocean as a homogeneous fluid, the APE discussed above is no longer applicable; however, in this case another form of GPE, the surface energy clearly stands out, and this energy is in connection with the free surface in the ocean. As shown in Section 2, the free surface elevation is energetically closely linked to the oceanic general circulation. In fact, for large-scale motions the slope of the sea surface elevation and the barotropic velocity are linked through the geostrophy constraint. Furthermore, in the stratified ocean, the free surface elevation anomaly is closely linked to the existence of the sloping main thermocline, and thus the APE.

As an example, Fig. 1 shows the climatological mean SSH from the GODAS data. Since the online GODAS data is based on an uneven grid of 1°×(1/3)° resolution, we convert it onto a dataset of 1°×1° resolution (converted GODAS data hereafter). There is a large north-south SSH difference between the subtropical gyres and the Southern Ocean, on the order of 2 m. As discussed by Wunsch (1998) and Huang (2010), this strong SSH front is directly associated with the zonal wind stress energy input to the Southern Ocean and the northward Ekman transport associated with the Southern Westerlies. If the wind stress over the Southern Ocean is weakened, the GPE associated with the SSH distribution, the ASPE, is released, and the adjustment ensures. Water in the subtropical gyres tends to move towards the Southern Ocean, reducing the slope of SSH across the fronts associated with Antarctic Circumpolar Current.

The amount of GPE stored in the system depends on the choice of reference. For the global scale or basin scale circulation, a globally flat sea surface can be used as the reference, i.e., $\overline{\eta} = 0$. According to Eq. (8), the SPE for a water column is $\chi_s = \frac{g\rho_0}{2}\eta^2$, and the corresponding total SPE in the world oceans is

$$\sum \chi_s = \frac{g\rho_0}{2} \iint \eta^2 \mathrm{d}x\mathrm{d}y. \quad (11)$$

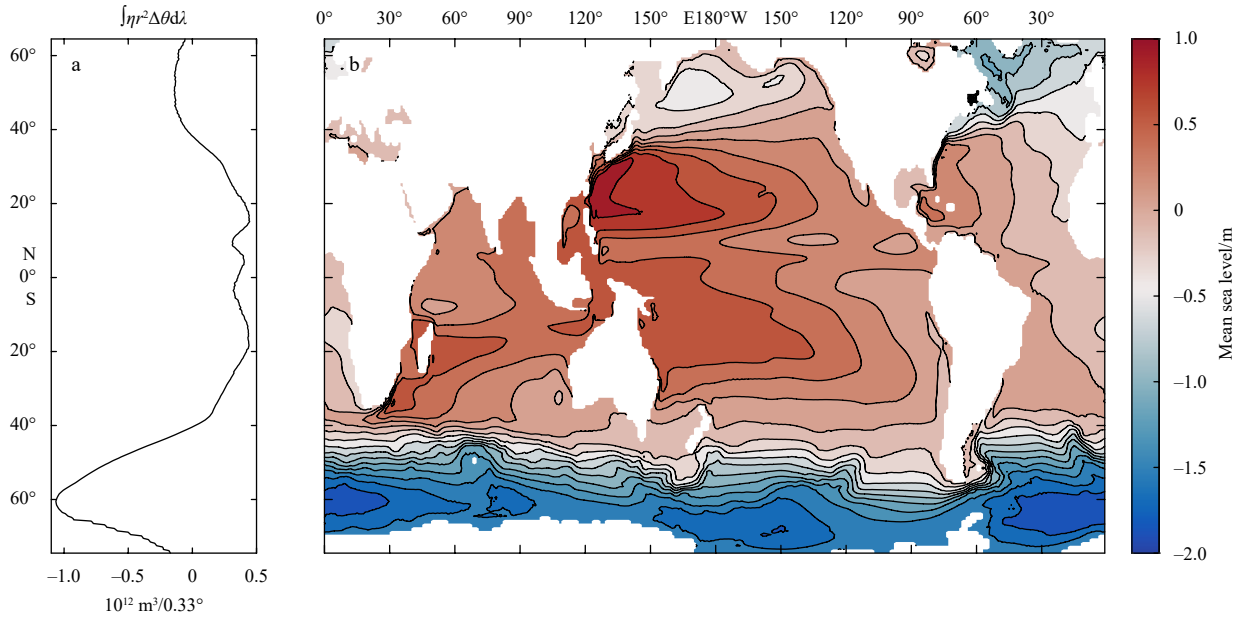The distribution of SPE in the world oceans is shown in Fig. 2.

Fig. 1. Climatological mean sea surface height in the world oceans, based on the converted Global Ocean Data Assimilation System data.
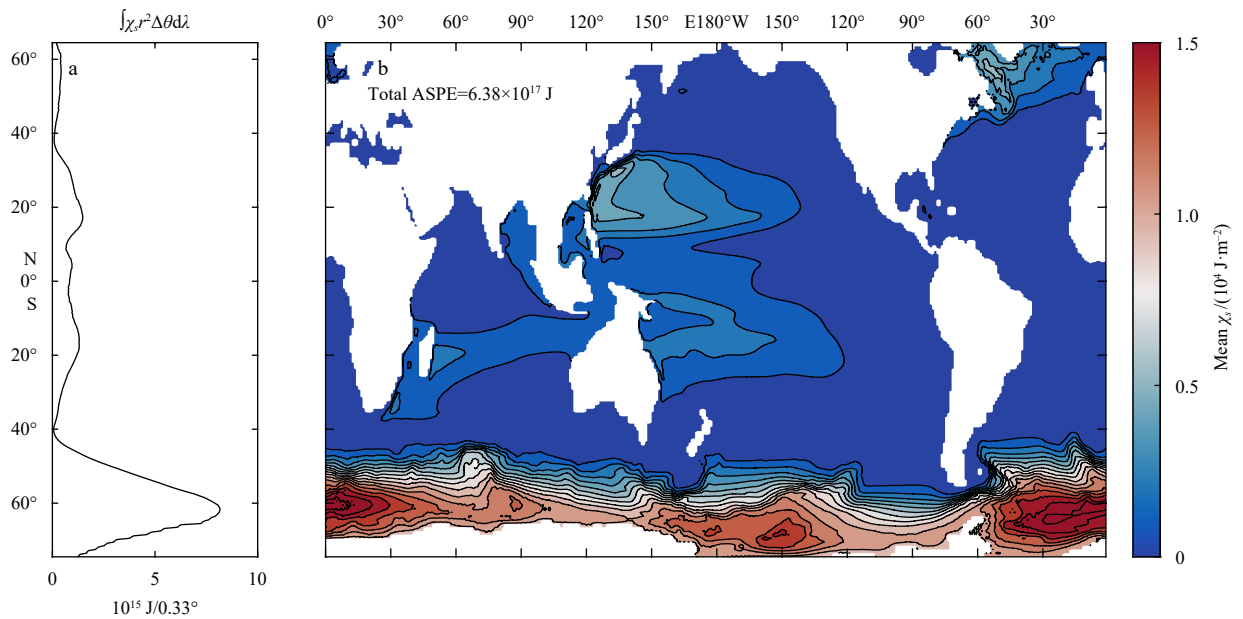

Fig. 2. Climatological mean available surface potential energy (ASPE) in the world oceans, based on the converted Global Ocean Data Assimilation System data.

The Southern Ocean is marked by the high SPE, which can be re-leased, if the global scale wind stress and the thermohaline for-cing are changed. The total amount of SPE in the world oceans is estimated at 6.38×10^{17} J, which is slightly smaller than the APE (1.00×10^{18} J) of the world oceans, based on the horizontal resolu-tion of 1°, as discussed by Huang (2010).

Although this amount of mechanical energy is quite large, its release or conversion to other forms of mechanical energy is quite limited, i.e., most of its part is not really available for main-taining other forms of motions in the ocean. Therefore, it is desir-able to examine part of this energy which can be converted to other forms of mechanical energy under common situations as discussed in the following section.

The essential point in definition Eq. (11) is the hidden as-sumption that the world oceans would adjust towards a state of a globally flat surface $\overline{\eta} = 0$. In reality, the global sea level is un-likely to flatten to such an extreme state. For practical situations, sea level adjustment is likely controlled by the sub-basin scales or mesoscales. Hence, the local mean sea level can be used as the reference state, and the corresponding variable is called the ASPE in this study.

The value of the ASPE at each grid point of a regular grid can be defined by the following 9-point scheme:

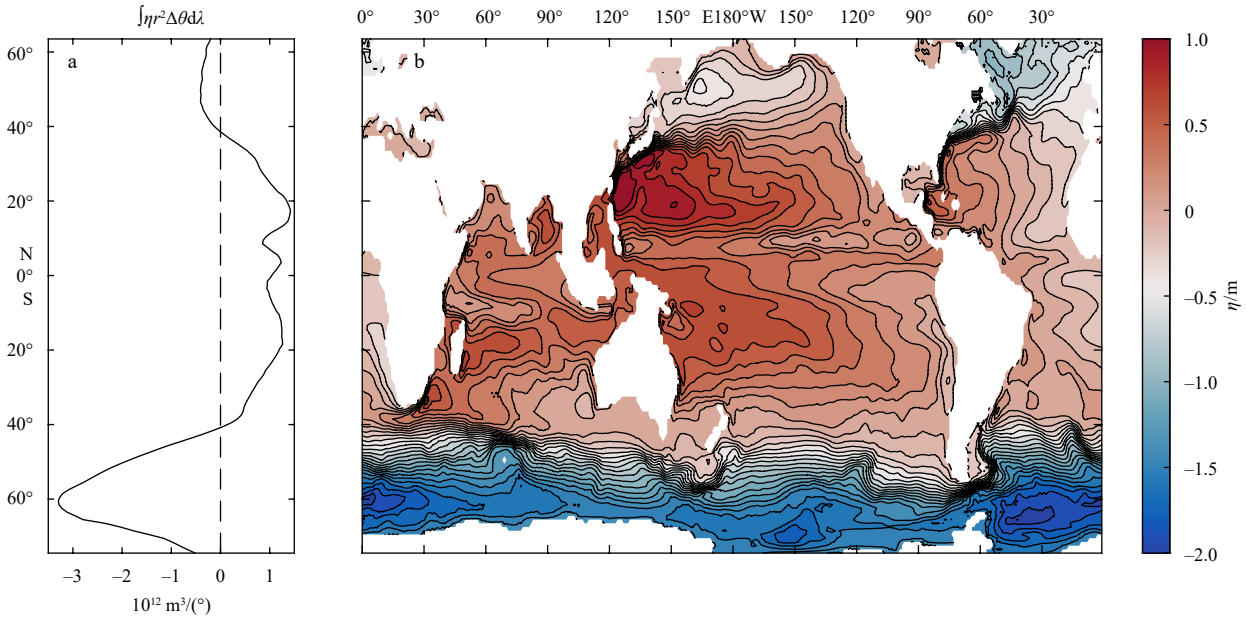$$\chi_{s,i,j} = \frac{g\rho_0}{2}\left(\eta_{i,j} - \overline{\eta_{i,j}}\right)^2, \tag{12}$$

Fig. 3. The global sea surface height in July 2003, based on the converted Global Ocean Data Assimilation System data.

where the $\overline{\eta_{i,j}}$ is defined as the local mean sea level over the 9 points.

The choice of a 9-point average is somewhat subjective. Obviously, one may choose other grid schemes, such as 4-point or 16-point schemes. However, they imply different horizontal scales, and thus different ASPE corresponding to such scales. Our discussion hereafter is based on a randomly chosen monthly mean SSH data of converted GODAS data for the period of July 2003.

The mean SSH field for July 2003 is shown in Fig. 3. Its feature is quite similar to the climatological mean SSH field shown in Fig. 1: there is high SSH in the subtropical basins and low SSH in the Southern Ocean and in the northern North Atlantic Ocean. There is also the C-shaped SSH structure in the western North Pacific Ocean, including rather strong gradient of SSH between the equator and 20°N. In addition, there are strong fronts in the northern edge of the Antarctic Circumpolar Current.

The corresponding monthly mean ASPE field is calculated based on the 9-point scheme of Eq. (12),

$$\sum \chi_s = \frac{g\rho_0}{2} \iint \left(\eta_{i,j} - \overline{\eta_{i,j}} \right)^2 \mathrm{d}x\mathrm{d}y. \tag{13}$$

As shown in Fig. 4, there are regions of high ASPE, including the western boundary currents before separation in each basin, such as the Gulf Stream, Kuroshio, Agulhas Current, East Australia Current, Malvinas Current, and most importantly the Antarctic Circumpolar Current. In the meridional direction, the regions of high ASPE appear around the latitude bands of 40°–60°S, 10°S, 10°N and 30°N, as shown in Fig. 4a. These regions of high ASPE is located near the bands of strong SSH fronts shown in Fig. 3.
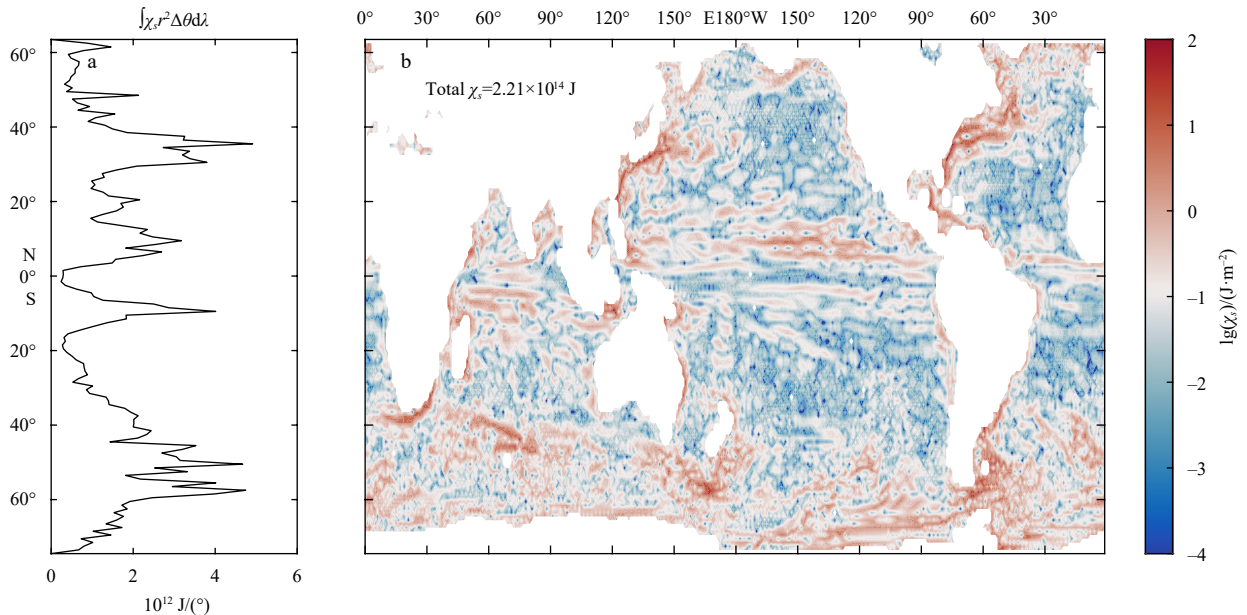

Fig. 4. The global available surface potential energy in July 2003, based on the converted Global Ocean Data Assimilation System data.
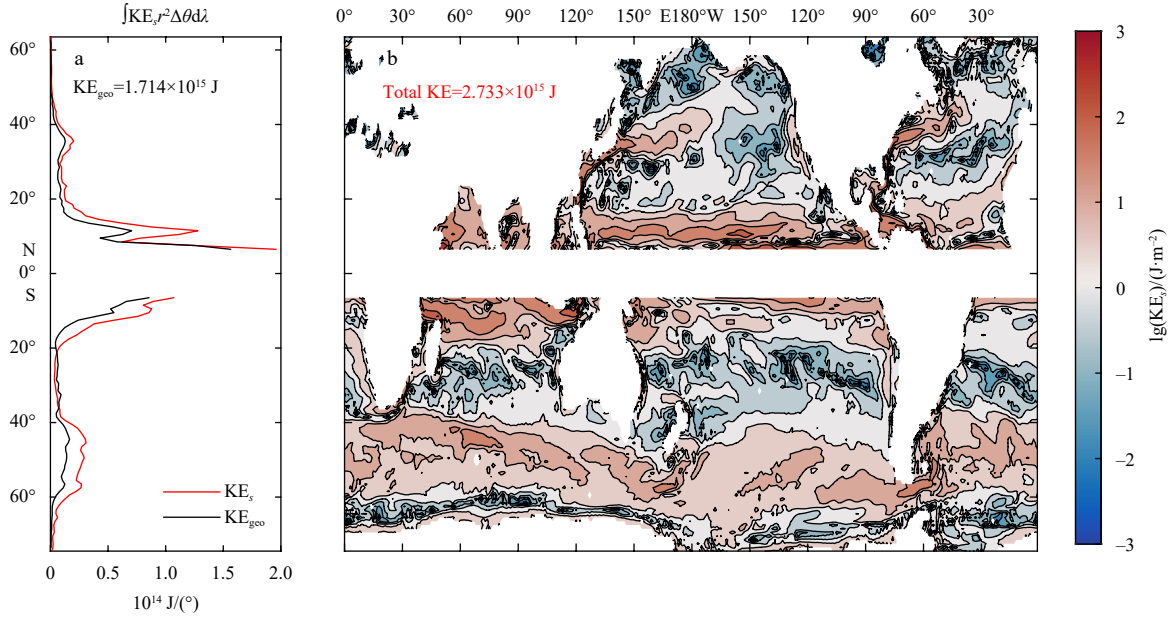
Fig. 5. The global surface kinetic energy (KE) in July 2003, based on the converted Global Ocean Data Assimilation System data.

Since the ASPE is potentially linked to the KE in the ocean, we first plot the surface KE, as shown in Fig. 5. The surface KE is defined by the horizontal velocity in the upmost layer (10 m thick), and its global scale distribution is somewhat similar to that of ASPE, but with a much smoother feature. In order to compare with KE obtained from the AVISO data, we also estimated the KE inferred from the geostrophic velocity inferred from the GODAS data by geostrophic approximation. Since geostrophy breaks down near the equator, we omit the contribution within the equatorial band (5°S–5°N). As shown in Fig. 5a, The KE associated with the total velocity from GODAS data is larger than the KE inferred from geostrophy because the velocity in the model ocean may include Ekman flow and wind-forced inertial motions.

As shown in Section 2, for a homogeneous ocean the SPE is directly linked to the KE associated with the barotropic velocity. Our following discussion is focused on eddies with horizontal scale of 100 km (1°×1°); therefore, we separate the total zonal

(meridional) velocity into the eddy component by first subtracting the climatological monthly mean zonal (meridional) velocity, and then the local background zonal (meridional) velocity, which is defined by the same 9-grid point mean similar to that shown in Eq. (12).

Afterwards, the EKE for each water column is separated into two components: the barotropic KE and the baroclinic KE.

$$\text{EKE}_{\text{BT}} = \frac{\rho_0}{2} \int_{-H}^{0} \left(u_{\text{BT}}^2 + v_{\text{BT}}^2 \right) \text{d}z, \ \ \text{EKE}_{\text{BC}} = \frac{\rho_0}{2} \int_{-H}^{0} \left(u_{\text{BC}}^2 + v_{\text{BC}}^2 \right) \text{d}z. \tag{14}$$

The corresponding monthly mean EKE distributions are shown in Figs 6b and c. In addition, we plot the meridional distribution of the zonally integrated ASPE and EKEs in Fig. 6a. The patterns of these three energy terms are somewhat similar in the subtropical and subpolar regions, suggesting some dynamic connection between these energy terms. However, within the 20° of
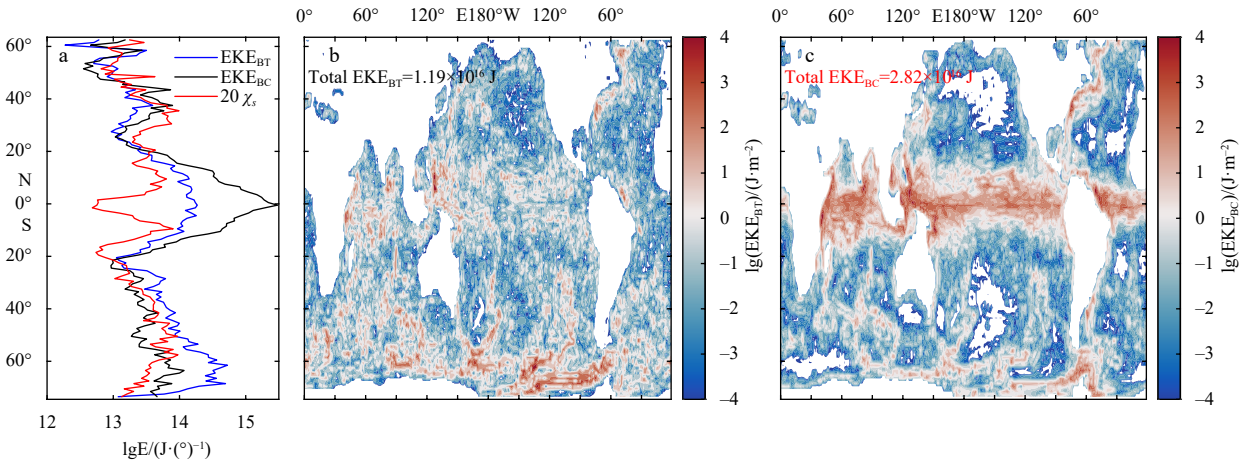

Fig. 6. The energy terms: a. the meridional distribution of EKE_{BT} and EKE_{BC} and available surface potential energy (multiplied by a factor of 20); b. the distribution of EKE_{BT}; c. the distribution of EKE_{BC} in July 2003, based on the converted Global Ocean Data Assimilation System data.

the equator, the meridional profiles of these energy terms are quite different, suggesting that they are regulated by different mechanisms.

Overall, in the equatorial band the EKE is dominated by the baroclinic energy. This is apparently related to the fact that there are multiple zonal jet-like features with east-west alternative flow directions in the equatorial band. As a result, in the equatorial region, EKE_{BT} is much smaller than the EKE_{BC}, Fig. 6a. For the global ocean, the total EKE_{BC} is 2.82×10^{16} J, more than 2 times of the total EKE_{BT} (1.19×10^{16} J), for July 2003. Although barotropic KE is relatively small, it is the dominating term in the strong boundary currents and in particular in the Southern Ocean (Fig. 6b). Both the ASPE and EKE_{BT} are strong in the Southern Ocean, as shown in Figs 5 and 6; this suggests a close dynamic link between these two variables in this region.

To examine the relative role of barotropic KE in the total KE, we also calculate the fraction of EKE_{BT} in the total EKE at each location, which is defined as $EKE_{BT}/\left(EKE_{BT} + EKE_{BC}\right)$. As shown in Fig. 7, for the most parts of the world oceans, barotropic energy is dominating. In fact, the zonal mean of barotropic energy fraction is larger than 0.5 for most latitude bands, except for the 20° tropical band, north of 50°N and a narrow band near Antarctica. This figure reflects the fact that for horizontal resolution of 1°, EKE in off-equatorial oceans is mostly dominated by the barotropic term.

The following subsection is focused on a latitude band of 57.5°–68.5°S. Over the entire 40 years of the GODAS data record the ASPE, EKE_{BT}, EKE_{BC} and wind stress (TAUX) within this latitudinal band went through great changes, Fig. 8. Most noticeably, ASPE, EKE_{BT} and EKE_{BC} reached their peaks around 2002–2004; on the other hand, zonal wind stress in this latitudinal band does not show such maximum. Therefore, at least in this latitudinal band, the maximum events in these three energy terms are not directly linked to the zonal wind stress anomalies. It seems that energetics of this latitudinal band may be affected by wind stress applied to a much broad latitudinal band of the Southern Ocean. It is to note that although the time series of EKE_{BT} and EKE_{BC} has rather similar features, both the mean value and standard devi-

ation of EKE_{BT} is several times larger than those of EKE_{BC}.

To explore the relationship between these variables, we plot their normalized seasonal cycles. As shown in Fig. 9, the normalized seasonal cycles of ASPE, EKE_{BT} and EKE_{BC} reach their maximum in September; both the seasonal cycles of ASPE and EKE_{BC} are quite similar to each other, with the corresponding minimum appears in February; however, the minimum of EKE_{BT} appears one month later. On the other hand, the seasonal cycle of the local zonal wind stress is noticeably different from the other three variables, suggesting that there is a phase difference between the seasonal cycles of these energy variations and that of the local zonal wind stress.

The relationship between these four terms is further explored by comparing their normalized time series, as shown in Figs 10 and 11. The normalized time series of ASPE, EKE_{BT} and EKE_{BC} have similar features, as shown in Fig. 10. In fact, the correlation coefficients between these time series are quite high, vary from 0.76, 0.70 to 0.83, all passing the 95% confidential level testing. This fact indicates that their variations are closely related. Apparently, the correlation is maximum with no lead-lag; for lead or lag on the order of six months, the correlation is minimum, as shown in Fig. 10d.

On the other hand, the correlation coefficients between the time series of TAUX with ASPE, EKE_{BT} and EKE_{BC} are much lower, although they all pass the 95% confidential level testing. Thus, the dynamic correlations between the zonal wind stress and the energetic terms, all integrated over this latitudinal band, are weak. Apparently, the correlation is close to maximum with no lead-lag; for lead or lag on the order of six months, the correlation is minimum, as shown in Fig. 11d.

As a comparison, the corresponding monthly mean APE field is defined as

$$\sum \chi_{bc} = \frac{g}{2} \iint \mathrm{d}x\mathrm{d}y \int_{-H}^{0} \frac{\left(\rho_{i,j} - \overline{\rho_{i,j}}\right)^2}{\partial \rho_\theta / \partial z} \mathrm{d}z, \qquad (15)$$
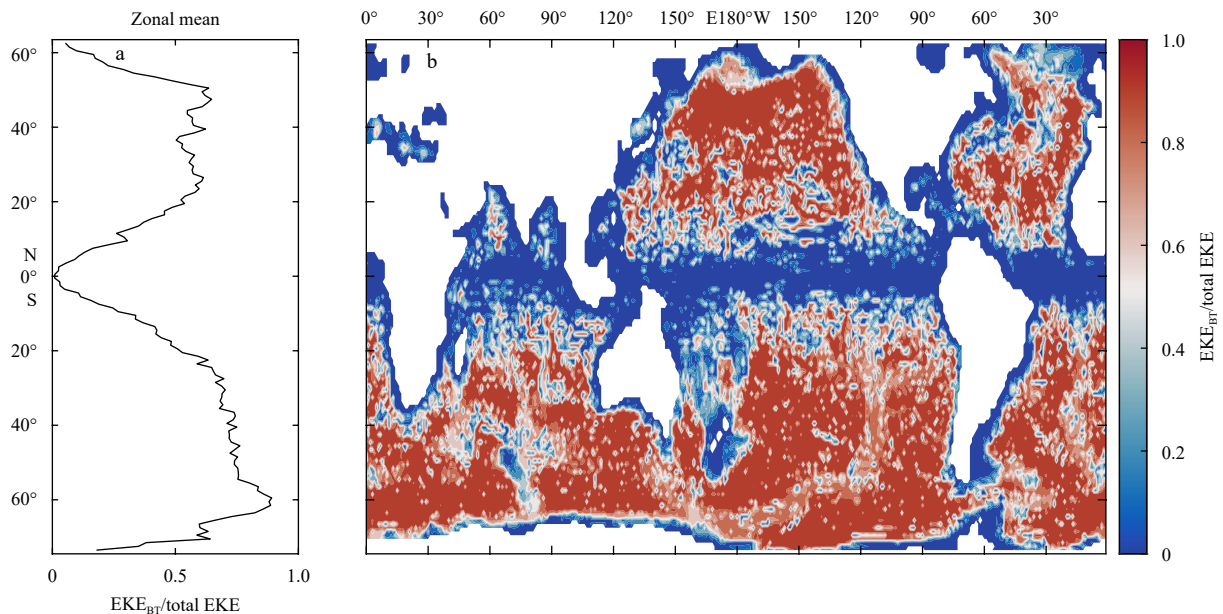

Fig. 7. The fraction of barotropic kinetic energy in the total kinetic energy in July 2003, based on the converted Global Ocean Data Assimilation System data.
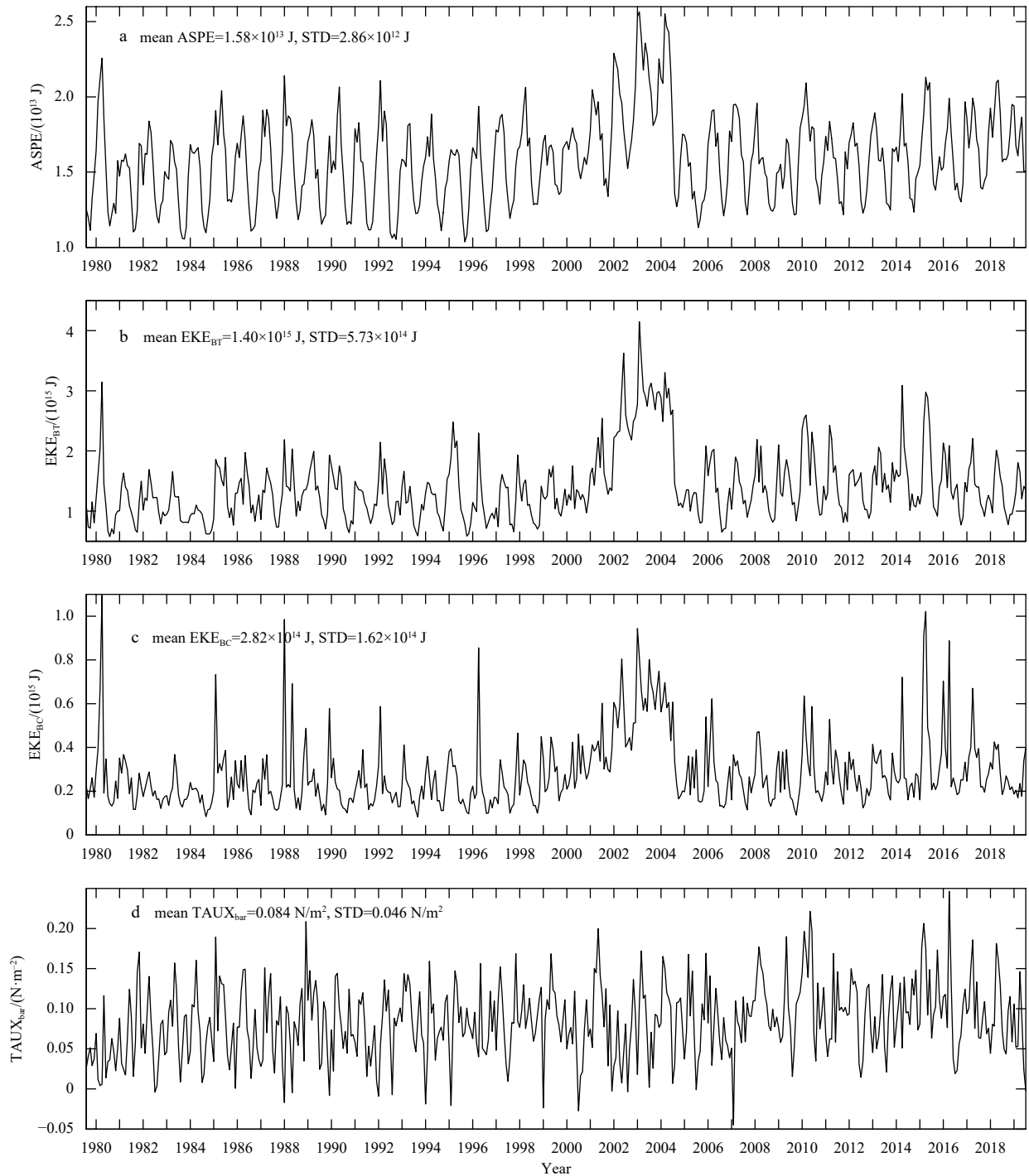
Fig. 8. Time series of energy integrated over the latitude band of 57.5°–68.5°S: a. ASPE; b. EKE_{BT}; c. EKE_{BC}; d. time series of zonal wind stress averaged over the latitude band of 57.5°–68.5°S, based on the converted Global Ocean Data Assimilation System data.

and the local mean density values $\overline{\rho_{i,j}}$ are calculated based on a 9-point scheme similar to Eq. (12); the local mean background stratification $\overline{\partial \rho_\theta / \partial z}$ is based on the potential density referred to the local pressure and calculated based on a 9-point scheme similar to Eq. (12); H is the total depth of the ocean at each grid point. The monthly mean field is shown in Fig. 12. If the integration is confined to the upper 1 000 m, the pattern and magnitude of APE remain roughly the same.

At this horizontal resolution there are four zonal bands of strong APE in the world oceans. The Antarctic Circumpolar Cur-

rent between 40°–60°S, the equatorial-extratropic band around 5°–15°N, the mid-latitude band around 25°–45°N, and the high latitude band around 60°N. These regions are closely linked to the strong currents and eddy activity in the world oceans, as discussed in many previous studies.

As discussed in Section 2, in the stratified ocean, the existence of ASPE and APE is dynamically linked to each other. It is clear that the bands of high APE in Fig. 12 are closely linked to the bands of high ASPE in Fig. 4. As shown in Eq. (7), the ASPE and EKE_{BT} can change due to the wind stress forcing in a homogen-
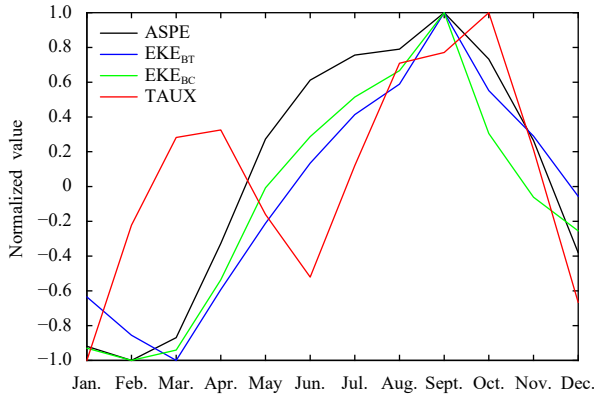
Fig. 9. Normalized seasonal cycle of ASPE, EKE_{BT}, EKE_{BC} and zonal wind stress (TAUX) over the latitude band of 57.5°–68.5°S, based on the converted Global Ocean Data Assimilation System data.

eous ocean. In addition, they are dynamically linked through the conservation of total energy, i.e., the conversion between ASPE and EKE_{BT}; such a dynamic link should also exist in the stratified ocean, as shown above. There is a third pathway of energy in the ocean, the barotropization—for spatial scale larger than the deformation radius, EKE tends to transfer toward larger scale two-dimensional flow, i.e., an energy flux from the baroclinic KE to the barotropic KE.

The connection between the SSH, ASPE and EKE is further explored using the AVISO satellite altimetry observations. Since our study is focused on large scale motions, the original AVISO data of 0.25° is converted to a data set of 1° resolution (converted AVISO data hereafter). As an example, the global SSH map for July 2003 from the converted AVISO data is shown in Fig. 13. Note that in comparison with Fig. 3, this map shows an overall similar structure, but with difference in details about the fine structure of SSH signals. This difference is likely due to many differences between these two types of SSH data. First, the GODAS data shown in Fig. 3 is the monthly mean SSH from the model, while the AVISO data is a monthly mean from the daily mean altimetry data. Nevertheless, the basic pattern is similar in these two figures and this reflects the basic dynamics in connection with the SSH in the real world and in the numerical simulations.

Using the SSH signals, the corresponding ASPE is calculated (Fig. 14), based on the same 9-point scheme in Eq. (14). In comparison, the AVISO data provide a picture of rather smoother distribution of the ASPE; in particular, there are broad regions of high ASPE associated with recirculation of both the Gulf Stream and the Kuroshio, plus the Agulhas Current, East Australia Current, Malvinas Current, and most importantly the Antarctic Circumpolar Current. The major difference between the ASPE calculated from GODAS (Fig. 4) and AVISO data exists for the near equatorial band of 10-degree off the equator, where the GODAS result shows quite strong ASPE, whereas the AVISO result shows virtually low energy within 20 degree off the equator. The reason for this difference is unclear at this time.

In order to calculate the KE on the upper ocean, the SSH signals are converted into the surface velocity, assuming geostrophy. Thereafter, the same 9-point scheme in Eq. (14) is used to calculate the EKE for the upper one meter of the ocean, Fig. 15. Since the geostrophic approximation is not valid near the equator, the zonal band of 5°S–5°N is excluded from this calculation. The global sum of ASPE for AVISO data is larger than the GODAS data.

In Fig. 15, regions of strong surface currents, such as the Gulf Stream, the Kuroshio, the Agulhas Current, the East Australia Current, the Malvinas Current, and the strong fronts in the Antarctic Circumpolar Current, are clearly shown as the regions of strong EKE. Comparing this figure with Fig. 14, it is detected that the regions of strong eddy activity are potentially linked to the regions of strong ASPE. In both the Gulf Stream and the Kuroshio, the range with a high surface KE calculated from the AVISO is much larger than that from the GODAS. This difference is likely because of the coarse horizontal resolution of the GODAS dataset missing many mesoscale eddies. Similarly, the high surface KE arising from active eddies (e.g., in the West Pacific subtropical ocean) is not shown in the GODAS data (Fig. 5) due to the coarse resolution. Despite these differences between the different datasets, the basic pattern of the high KE is roughly consistent with the ASPE in both the numerical simulations and satellite observations, reflecting that the ASPE is closely in connection with the KE of the oceanic circulation.

For the intra-seasonal timescale, the regions with a potential coherence between the ASPE and surface KE are mostly located over the low latitude band, Gulf Stream, Kuroshio extension, Northwest Pacific subtropical counter-current, and the Antarctic Circumpolar Current (Fig. 16). The spatial distribution of this intra-seasonal correlation is roughly in agreement with the global high ASPE and surface KE (Figs 14 and 15).

At the same time, we randomly choose four stations (depicted as blue stars in Fig. 16) in the Gulf Stream, Kuroshio extension, Northwest Pacific subtropical counter-current, and the Antarctic Circumpolar Current. The time series of the ASPE and surface KE are shown in Fig. 17; the correlation coefficients of ASPE and KE at these stations on intra-seasonal timescales are around 0.5. Together with the approximately seasonal coherence (Figs 8 and 9), these results indicate that the ASPE postulated in this study is likely an important energetic quantity and potentially linked to the oceanic KE in the upper ocean.

As shown in Table 1, the global sum of ASPE and surface KE for both the GODAS and AVISO data are comparable. ASPE diagnosed from AVISO is about three times as large as that from GODAS. There are differences between these two datasets. Maps from the AVISO data are based on the 1°×1° daily mean. On the other hand, maps from the converted GODAS data are based on the 1°×1° monthly mean; thus, with numerical smoothing, many fine features of the SSH anomaly are wiped out. Nevertheless, these figures roughly show that in the world oceans ASPE and EKE are linked to each other.

Additionally, based on a ~7.5 km-resolution ROMS simulation data (Jing et al., 2021), we also preliminarily examine the regional ASPE and surface KE in the eddy-active Northwest Pacific Ocean, as well as their potential connection. Shown in Figs S5–S14 for both the scales of <20 km and >50 km, the basic pat-

Table 1. The sum of available surface potential energy (ASPE), surface kinetic energy (KE) and eddy kinetic energy (EKE) (unit : J) of Global Ocean Data Assimilation System (GODAS) and AVISO data

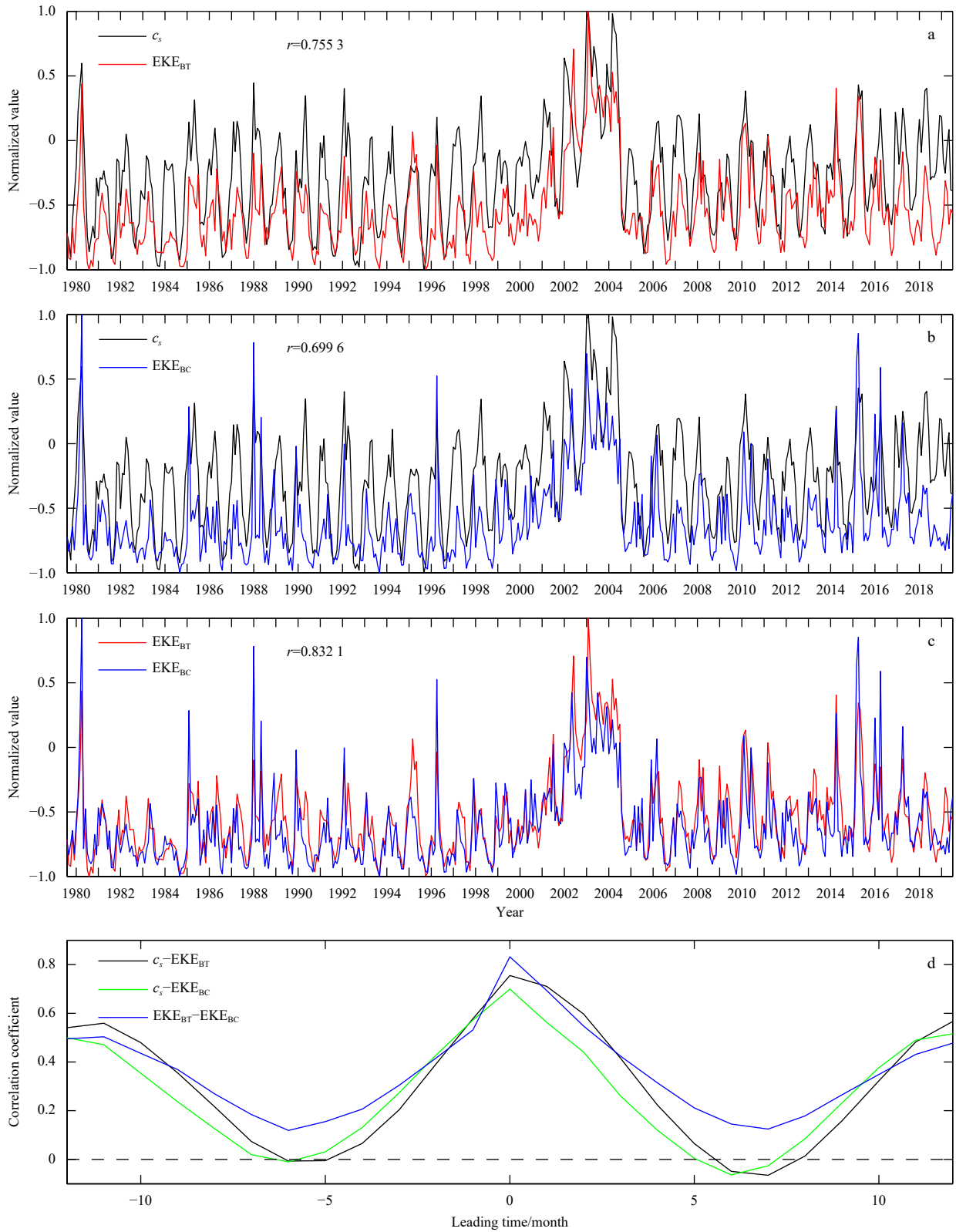| Data set		ASPE	Surface KE	Total EKE	
				EKE_{BT}	EKE_{BC}
GODAS	global (July, 2003)	2.21×10^{14}	2.73×10^{15}	1.19×10^{16}	2.82×10^{16}
	57.5°–68.5°S (multi-year mean)	1.58×10^{13}	–	1.40×10^{15}	2.82×10^{14}
AVISO	global (July, 2003)	5.31×10^{14}	7.36×10^{15}	–	–

Note: – represents no data.

Fig. 10. Time series of the normalized energy integrated over the latitude band of 57.5°–68.5°S and their correlations, based on the converted Global Ocean Data Assimilation System data. a. ASPE vs. EKE$_{BT}$; b. ASPE vs. EKE$_{BC}$; c. EKE$_{BT}$ vs. EKE$_{BC}$; d. lead-lag correlation.

terns of high ASPE and surface KE are roughly consistent with those in both the GODAS data and the AVSIO altimetry observations. The strong signals of ASPE and surface KE are mostly loc-

ated in the Kuroshio extension and subtropical counter-current (STCC) regions, presumably associated with the boundary current baroclinic instability and active mesoscale eddies. Their sea-
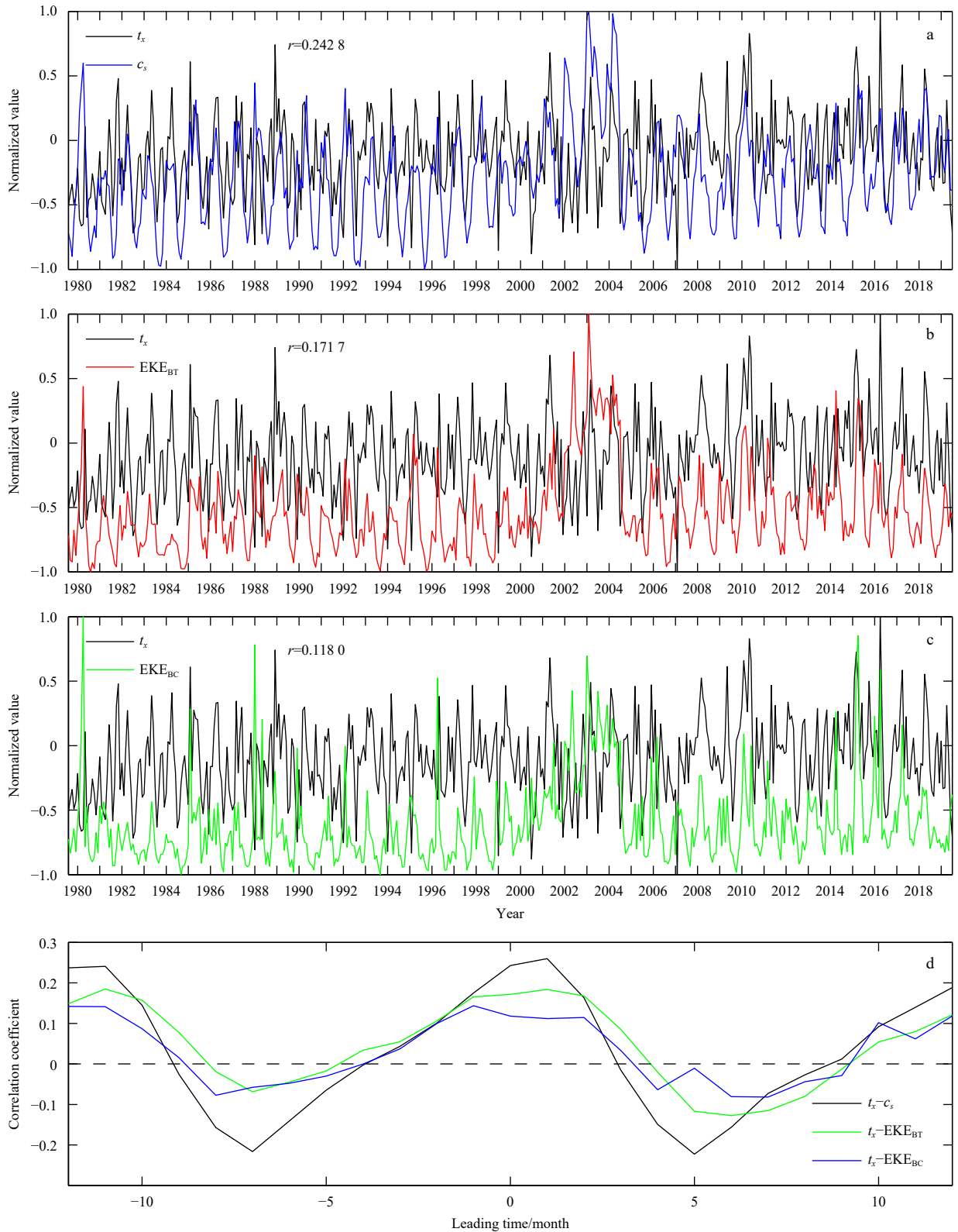
Fig. 11. Time series of the normalized zonal wind stress and energy terms and their correlations (integrated over the latitude band of 57.5°–68.5°S, based on the converted Global Ocean Data Assimilation System data). a. TAUX vs. ASPE; b. TAUX vs. KE$_{BT}$; c. TAUX vs. EKE$_{BC}$; d. lead-lag correlation.

sonal variations are similar with the results from the converted GODAS data. For the scale <20 km (Figs S5–S9), the enhanced ASPE tends to be aligned with the high surface KE, mostly locat-

ing at the Kuroshio extension region and the periphery of meso-scale eddies. This result is indicative of a potential dynamical connection between the ASPE and the KE of mesoscale eddies. At
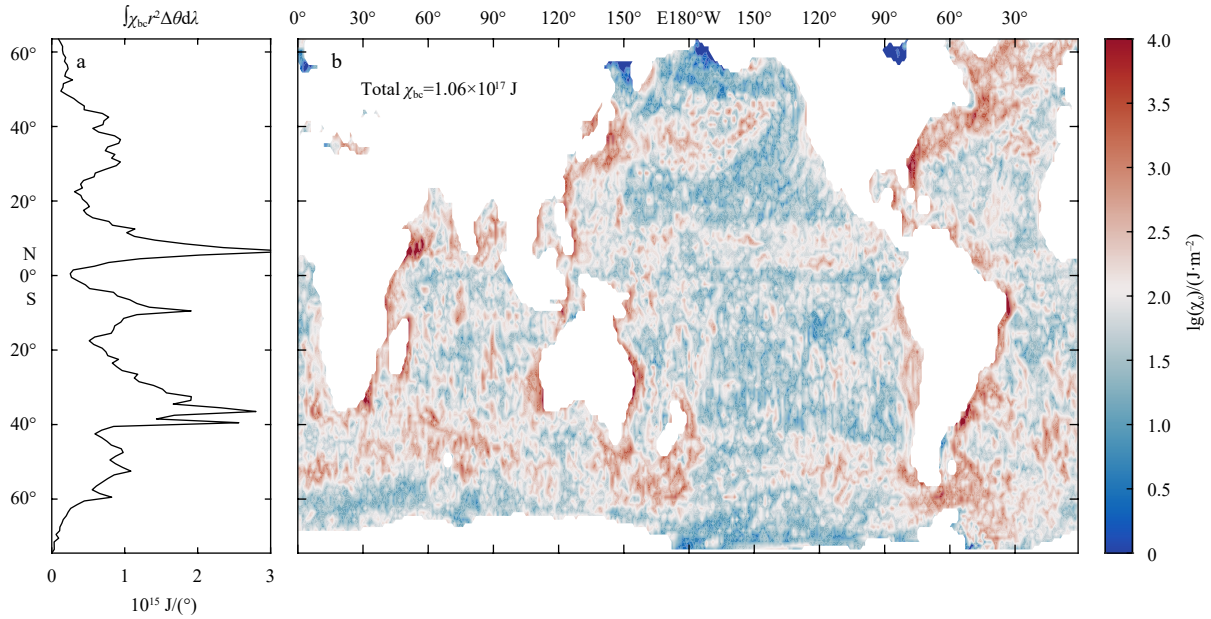
Fig. 12. The global available potential energy in July 2003, based on the converted Global Ocean Data Assimilation System data.
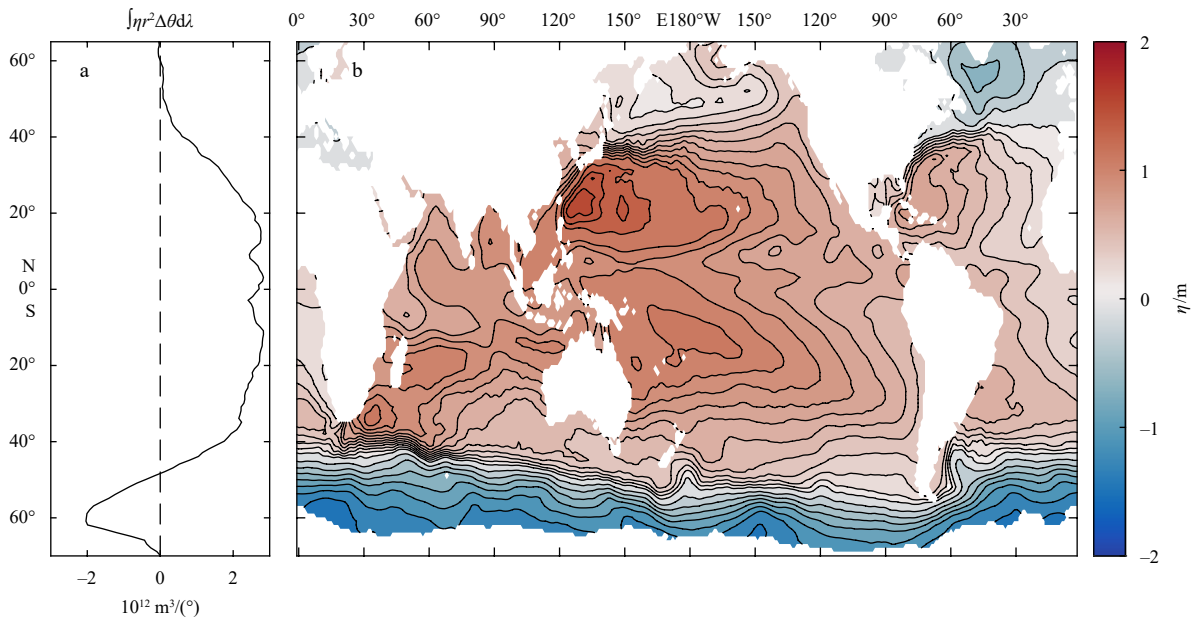
Fig. 13. The global sea surface height in July 2003, based on the converted AVISO data.

the same time, the ratio of ASPE vs. KE at the scale <20 km (~0.26) is higher than that at the scale >50 km (~0.15), implying the ASPE linked to KE containing more important signals within smaller-scales (e.g., submesoscales). In addition, for the scale <20 km in the Kuroshio extension (28°–38°N, 140°–165°E), the correlation coefficients between the ASPE and two EKE components (EKE_{BT}, EKE_{BC}) are 0.94 and 0.92, separately (Fig. S8), which are higher than those in the scale >50 km (Fig. S13). Similar result also exists in the eddy-active STCC region (15°–25°N, 125°–165°E) and suggests a likely more close connection between ASPE and surface KE at the smaller-scales.

The main purpose of this paper is to introduce the concept of ASPE and here the application of ASPE is preliminary, partly due to the absence of finer-scale altimeter data at this time. The spe-

cific application of the ASPE and its detailed dynamical connection with other energetic terms, especially for smaller-scale ageostrophic processes, still need further investigation in the future.

4 Conclusions

Surface elevation is an important dynamical variable in the oceanic circulation. Over the past decades, satellite altimetry observations have provided a wealth of sea surface elevation data, which have been analyzed in terms of the geostrophic velocity inferred from the data including the horizontal wave number spectrum and the power spectrum of the equivalent geostrophic velocity field. The upcoming SWOT mission will provide snapshots of the global SSH with even higher horizontal resolution, and such surface elevation data will contain many dynamical signals other
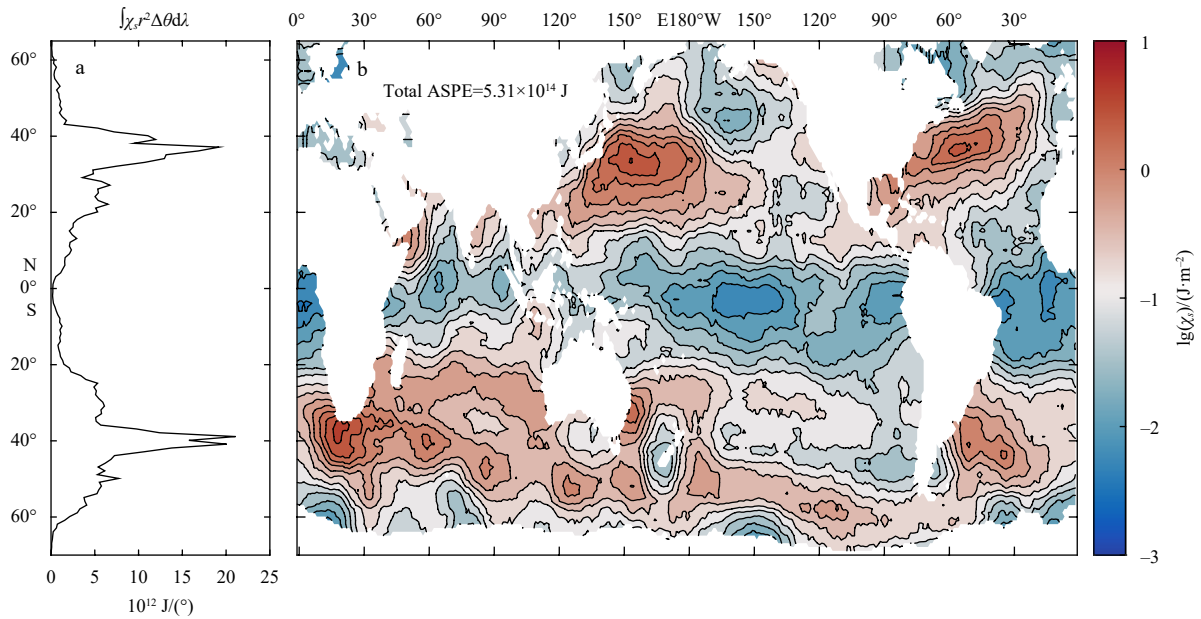
Fig. 14.　The global available surface potential energy (ASPE) in July 2003, based on the converted AVISO data.
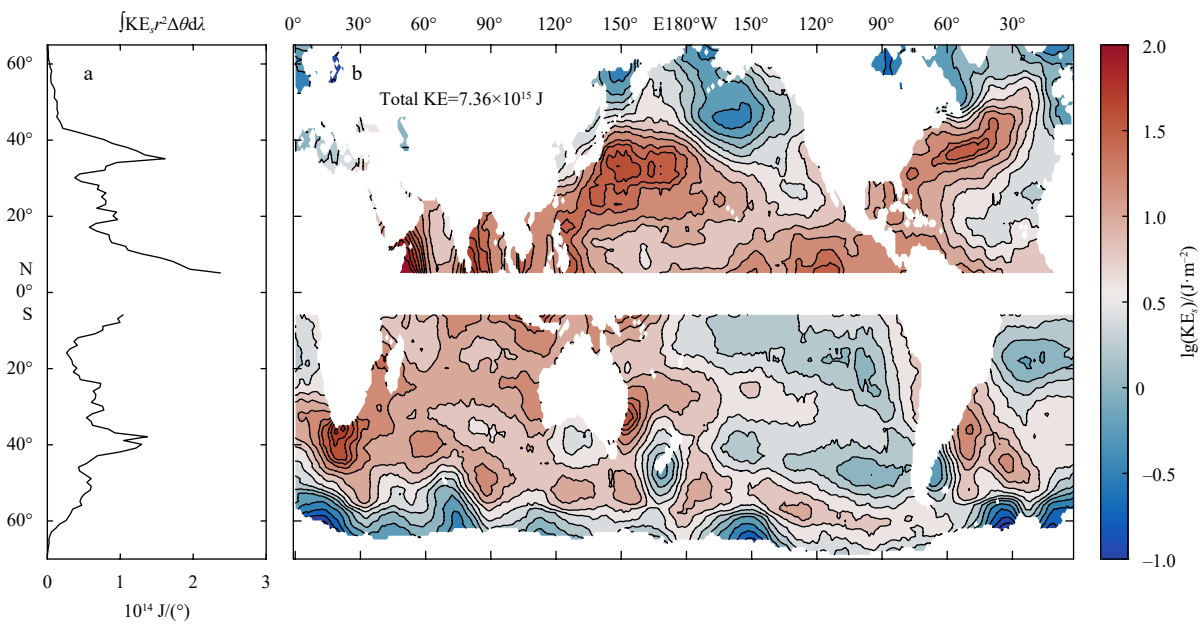

Fig. 15.　The global surface kinetic energy (KE) in July 2003, based on the converted AVISO data.

than the geostrophic velocity; thus, a direct diagnostic physical quantity independent of the geostrophy is likely useful.

In this study, a new concept, the available surface potential energy, is introduced for the dynamical description of the oceanic general circulation, defined as the density multiplied by half of the squared deviation from the local mean reference surface elevation. This concept is preliminarily applied to both the GODAS data and the AVISO data. The results indicate the links between ASPE and EKE in the ocean; furthermore, there is also a close link between the ASPE and APE in the ocean.

ASPE postulated in this study is an important energetic quantity, which is linked to the oceanic circulation in the upper ocean. Although our discussion in this study is mostly focused on the SSH data generated from numerical models or collected from

satellite observations, the concept of ASPE can be potentially applied to the SSH data collected from other means, from global tidal gauges, surface radar from airplanes and other instruments. Furthermore, the mechanical energy associated with the free surface of the ocean may be an important dynamic variable which can be used in other studies. Since ASPE is a quadratic quantity, this raises a theoretical question whether the ASPE can be partitioned into the corresponding components associated with geostrophic currents, internal waves, surface waves and turbulence. Although we have presented some theoretical analysis for this new quantity in Section 2 and in supplementary materials, our analysis related to velocity field is based on geostrophy; thus, the situations related to unbalanced motions for horizontal scales smaller than the first baroclinic radius of deformation are left for
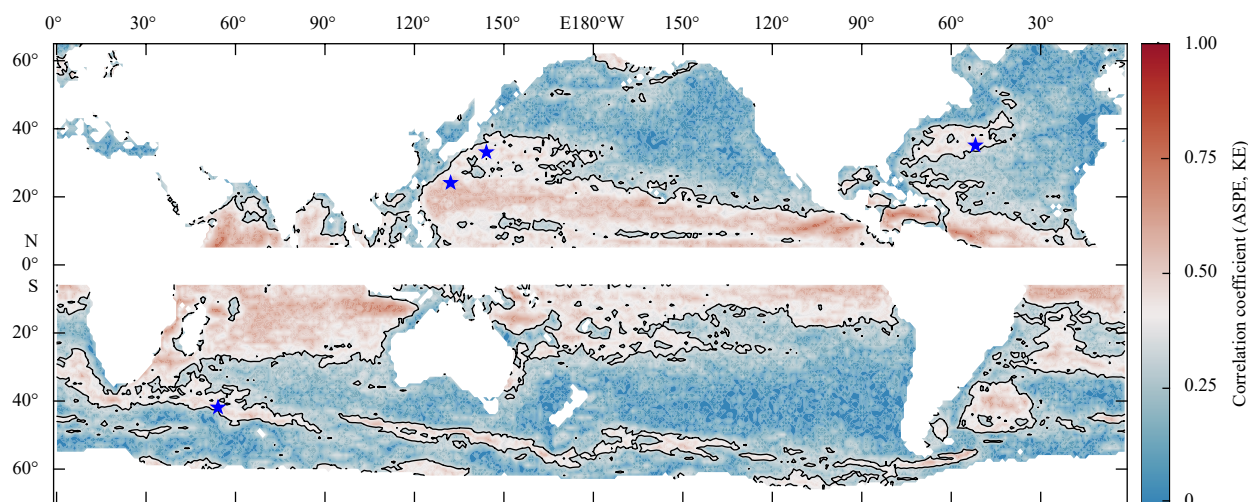
Fig. 16. The correlation coefficient between global available surface potential energy (ASPE) and surface kinetic energy (KE) within the intra-seasonal timescale, based on the daily AVISO data of 2000–2016 and a 30–120 days band-pass filtering.
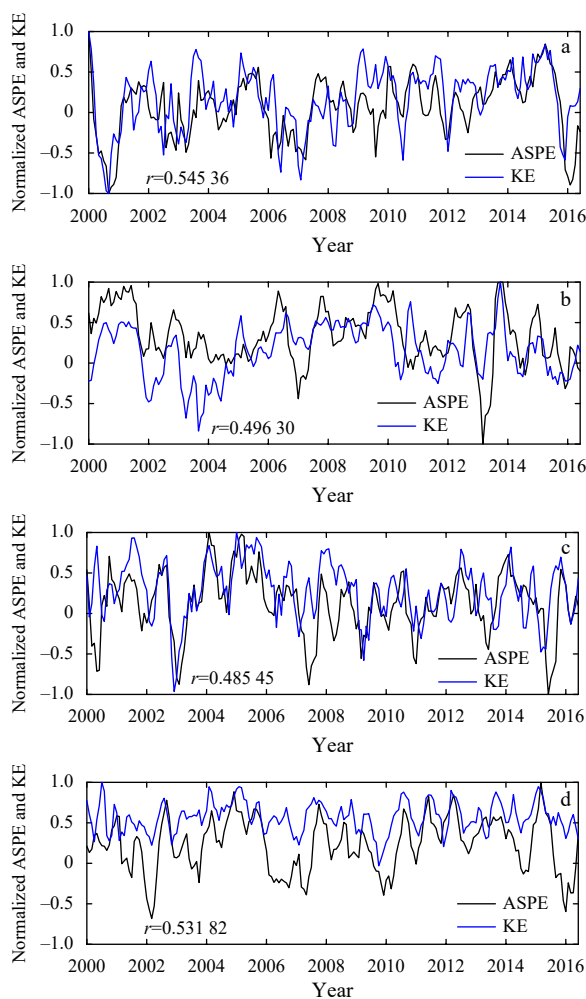

Fig. 17. Intra-seasonal time series of the available surface potential energy (ASPE) and surface kinetic energy (KE) and their correlations at four randomly chosen points (as blue stars shown in Fig. 16) in the Gulf Stream (a), Kuroshio extension (b), Northwest Pacific subtropical counter-current (c), and the Antarctic Circumpolar Current (d), based on the daily AVISO data of 2000–2016 and a 30–120 days band-pass filtering.

further study. Since ASPE can be defined for a large range of spatial and temporal scales, it is clear that much more study is needed in both theory and application based on this dynamical quantity. For example, Wang and Huang (2004) estimated of the wind stress energy input to the surface waves in the world oceans at 60 TW. According to the classic theory of surface waves, the potential energy and kinetic energy is equally partitioned over the wave length (Mei, 1983); thus, ASPE may play a more important role, if we enter the region of surface waves, on the order of 100 m. The energetics of ASPE for such a length scale poses a grand challenge.

Acknowledgements

References

Apel J R. 1980. Satellite sensing of ocean surface dynamics. Annual Review of Earth and Planetary Sciences, 8: 303–342, doi: 10.1146/annurev.ea.08.050180.001511

Apel J R, Byrne H M, Proni J R, et al. 1975. Observations of oceanic internal and surface waves from the earth resources technology satellite. Journal of Geophysical Research, 80(6): 865–881, doi: 10.1029/JC080i006p00865

Apel J R, Byrne H M, Proni J R, et al. 1976. A study of oceanic internal waves using satellite imagery and ship data. Remote Sensing of Environment, 5: 125–135, doi: 10.1016/0034-4257(76)90043-2

Behringer D, Xue Yan. 2004. Evaluation of the global ocean data assimilation system at NCEP: The Pacific Ocean. In: Eighth Symposium on Integrated Observing and Assimilation Systems for Atmosphere, Oceans, and Land Surface, AMS 84th Annual Meeting. Washington: Washington State Convention and Trade Center, 11–15

Blumen W. 1972. Geostrophic adjustment. Reviews of Geophysics, 10(2): 485–528, doi: 10.1029/RG010i002p00485

Cao Haijin, Jing Zhiyou, Fox-Kemper B, et al. 2019. Scale transition from geostrophic motions to internal waves in the northern South China Sea. Journal of Geophysical Research: Oceans, 124(12): 9364–9383, doi: 10.1029/2019jc015575

Chavanne C P, Klein P. 2010. Can oceanic submesoscale processes be observed with satellite altimetry?. Geophysical Research Let-

ters, 37(22): L22602, doi: 10.1029/2010gl045057

Chelton D B, Schlax M G, Samelson R M, et al. 2019. Prospects for future satellite estimation of small-scale variability of ocean surface velocity and vorticity. Progress in Oceanography, 173: 256–350, doi: 10.1016/j.pocean.2018.10.012

Ferrari R, Wunsch C. 2009. Ocean circulation kinetic energy: reservoirs, sources, and sinks. Annual Review of Fluid Mechanics, 41(1): 253–282, doi: 10.1146/annurev.fluid.40.111406.102139

Frederikse T, Landerer F, Caron L, et al. 2020. The causes of sea-level rise since 1900. Nature, 584(7821): 393–397, doi: 10.1038/s41586-020-2591-3

Gill A E. 1982. Atmosphere-Ocean Dynamics. New York: Academic Press, 30

Gula J, Molemaker M J, McWilliams J C. 2014. Submesoscale cold filaments in the gulf stream. Journal of Physical Oceanography, 44(10): 2617–2643, doi: 10.1175/jpo-d-14-0029.1

Huang Ruixin. 2005. Available potential energy in the world's oceans. Journal of Marine Research, 63(1): 141–158, doi: 10.1357/0022240053693770

Huang Ruixin. 2010. Ocean Circulation: Wind-Driven and Thermohaline Processes. Cambridge: Cambridge University Press, 791

Huang Ruixin, Jin Xiangze. 2002. Sea surface elevation and bottom pressure anomalies due to thermohaline forcing. Part I: isolated perturbations. Journal of Physical Oceanography, 32(7): 2131–2150, doi: 10.1175/1520-0485(2002)032<2131:sseabp>2.0.co;2

Jing Zhiyou, Fox-Kemper B, Cao Haijin, et al. 2021. Submesoscale fronts and their dynamical processes associated with symmetric instability in the Northwest Pacific Subtropical Ocean. Journal of Physical Oceanography, 51(1): 83–100, doi: 10.1175/JPO-D-20-0076.1

Klymak J M, Shearman R K, Gula J, et al. 2016. Submesoscale streamers exchange water on the north wall of the Gulf Stream. Geophysical Research Letters, 43(3): 1226–1233, doi: 10.1002/2015gl067152

Lorenz E N. 1955. Available potential energy and the maintenance of the general circulation. Tellus, 7(2): 157–167, doi: 10.3402/tellusa.v7i2.8796

Mahadevan A. 2016. The impact of submesoscale physics on primary productivity of plankton. Annual Review of Marine Science, 8(1): 161–184, doi: 10.1146/annurev-marine-010814-015912

Margules M. 1905. Uber die energie der sturme. Wein K K. Hof-und. Stattsdruckerei: 26

Mei C C. 1983. The Applied Dynamics of Ocean Surface Waves. New York: Wiley, 740

Oort A H, Anderson L A, Peixoto J P. 1994. Estimates of the energy cycle of the oceans. Journal of Geophysical Research: Oceans, 99(C4): 7665–7688, doi: 10.1029/93jc03556

Oort A H, Ascher S C, Levitus S, et al. 1989. New estimates of the available potential energy in the world ocean. Journal of Geophysical Research: Oceans, 94(C3): 3187–3200, doi: 10.1029/JC094iC03p03187

Pedlosky J. 1987. Geophysical Fluid Dynamics. New York: Springer-Verlag, 710

Qiu Bo, Chen Shuiming, Klein P, et al. 2018. Seasonality in transition scale from balanced to unbalanced motions in the world ocean. Journal of Physical Oceanography, 48(3): 591–605, doi: 10.1175/jpo-d-17-0169.1

Qiu Bo, Nakano T, Chen Shuiming, et al. 2017. Submesoscale transition from geostrophic flows to internal waves in the northwestern Pacific upper ocean. Nature Communications, 8(1): 14055, doi: 10.1038/ncomms14055

Ray R D, Zaron E D. 2011. Non-stationary internal tides observed with satellite altimetry. Geophysical Research Letters, 38(17): L17609, doi: 10.1029/2011gl048617

Reid R O, Elliott B A, Olson D B. 1981. Available potential energy: a clarification. Journal of Physical Oceanography, 11(1): 15–29, doi: 10.1175/1520-0485(1981)011<0015:apeac>2.0.co;2

Su Zhan, Wang Jinbo, Klein P, et al. 2018. Ocean submesoscales as a key component of the global heat budget. Nature Communications, 9: 775, doi: 10.1038/s41467-018-02983-w

Sullivan P P, McWilliams J C. 2018. Frontogenesis and frontal arrest of a dense filament in the oceanic surface boundary layer. Journal of Fluid Mechanics, 837: 341–380, doi: 10.1017/jfm.2017.833

Taylor J R, Ferrari R. 2011. Ocean fronts trigger high latitude phytoplankton blooms. Geophysical Research Letters, 38(23): L23601, doi: 10.1029/2011gl049312

Thomas L N, Taylor J R, D'Asaro E A, et al. 2016. Symmetric instability, inertial oscillations, and turbulence at the Gulf Stream front. Journal of Physical Oceanography, 46(1): 197–217, doi: 10.1175/jpo-d-15-0008.1

Wang Wei, Huang Ruixin. 2004. Wind energy input to the surface waves. Journal of Physical Oceanography, 34(5): 1276–1280, doi: 10.1175/1520-0485(2004)034<1276:weitts>2.0.co;2

Wunsch C. 1998. The work done by the wind on the oceanic general circulation. Journal of Physical Oceanography, 28(11): 2332–2340, doi: 10.1175/1520-0485(1998)028<2332:twdbtw>2.0.co;2

Zhao Zhongxiang. 2017. The global mode-1 S_2 internal tide. Journal of Geophysical Research: Oceans, 122(11): 8794–8812, doi: 10.1002/2017jc013112

Supplementary information:

Fig. S1. The Rossby problem for a homogeneous ocean with an initial velocity jet (looking toward the east).

Fig. S2. Geostrophic adjustment induced by an initial step in sea surface elevation.

Fig. S3. Adjustment of an initial step of finite width of free surface elevation.

Fig. S4. Sketch of the model ocean.

Fig. S5. The Northwest Pacific SSH in the scale of <20 km (roughly following a 3-point scheme), July 15, 2003, based on the converted ROMS data.

Fig. S6. The Northwest Pacific ASPE in the scale of <20 km, July 15, 2003, based on the converted ROMS data.

Fig. S7. The Northwest Pacific surface KE in the scale of <20 km, July 15, 2003, based on the converted ROMS data.

Fig. S8. Normalized seasonal cycle of ASPE, EKE_{BT}, EKE_{BC} and zonal wind stress in the scale of <20 km over the Kuroshio extension region, based on the converted ROMS data. The correlation coefficients between the ASPE and two EKE components (EKE_{BT}, EKE_{BC}) are 0.94 and 0.92, separately.

Fig. S9. Normalized seasonal cycle of ASPE, EKE_{BT}, EKE_{BC} and zonal wind stress in the scale of <20 km over the STCC region, based on the converted ROMS data. The correlation coefficients between the ASPE and two EKE components (EKE_{BT}, EKE_{BC}) are 0.81 and 0.86, separately.

Fig. S10. The Northwest Pacific SSH in the scale of >50 km (roughly following a 7-point scheme), July 15, 2003, based on the converted ROMS data.

Fig. S11. The Northwest Pacific ASPE in the scale of >50 km, July 15, 2003, based on the converted ROMS data.

Fig. S12. The Northwest Pacific surface KE in the scale of >50 km, July 15, 2003, based on the converted ROMS data.

Fig. S13. Normalized seasonal cycle of ASPE, EKE_{BT}, EKE_{BC} and zonal wind stress in the scale of >50 km over the Kuroshio extension region, based on the converted ROMS data. The correlation coefficients between the ASPE and two EKE components (EKE_{BT}, EKE_{BC}) are 0.28 and 0.71, separately.

Fig. S14. Normalized seasonal cycle of ASPE, EKE_{BT}, EKE_{BC} and zonal wind stress in the scale of >50 km over the STCC region, based on the converted ROMS data. The correlation coefficients between the ASPE and two EKE components (EKE_{BT}, EKE_{BC}) are 0.40 and 0.78, separately.

The supplementary information is available online at https://10.1007/s13131-021-1852-9 and www.aosocean.com. The supplementary information is published as submitted, without typesetting or editing. The responsibility for scientific accuracy and content remains entirely with the authors.